ADVANCED FUNCTIONAL MATERIALS
www.afm-journal.de

Self-Recoverable, Highly Repeatable, and Thermally Stable Mechanoluminescence for Dual-Mode Information Storage and Photonic Skin Applications

Shiye Qin, Wanyuan Wei, Birong Tian, Zhidong Ma, Shaofan Fang, Yongsheng Wang, Jiachi Zhang,* and Zhaofeng Wang**

Mechanically driven light generation is an intriguing phenomenon holding great promise in various fields. However, the existing mechanoluminescence (ML) materials always suffer from poor self-recoverability, low repeatability, and environmental disturbance, severely hindering their practical applications. In this work, a self-activating ML system based on interfacial triboelectrification is created by compositing the $Ca_6BaP_4O_{17}$:0.02Ce^{3+} powders into a flexible polydimethylsiloxane (PDMS) matrix. With no need for pre-irradiation, the composite film emits self-activating and self-charging ML simultaneously in response to the rubbing or stretching stimuli. Accordingly, the $Ca_6BaP_4O_{17}$:0.02Ce^{3+}/PDMS exhibits desirable self-recovery and repeatable ML performance, which could still be recorded (or observed by naked eyes) even after ca. 1000 stretching cycles with a fast self-recovery period of < 0.1 s. Furthermore, the $Ca_6BaP_4O_{17}$:0.02Ce^{3+}/PDMS possesses good thermal stability in a temperature range from 298 to 473 K. The developed $Ca_6BaP_4O_{17}$:0.02Ce^{3+}/PDMS is applicable to various fields, and the dual-mode information storage and photonic skin devices are created as representatives. Compared to the existing oxide-based ML materials (the ML signal disappears after only several or tens of rapid mechanics cycles), this work breaks through the bottleneck issues on the self-recoverability, repeatability, and thermal stability, which significantly advances the ML field.

1. Introduction

Mechanoluminescence (ML) refers to the phenomenon that materials could emit light under mechanical stimuli such as fracture, friction, compression, grinding, and stretching.[1–10] The unique mechanics-optics conversion characteristics endow ML with remarkable advantages. On one hand, the incidental energy in human activities (e.g., machine operation, human motions, etc.) and the extensively existing energy in nature (e.g., wind energy, tidal energy, etc.) could be employed as stimulus resources to produce luminescence.[11–14] Therefore, ML shows high application prospects in the development of the new generation of lighting, displaying, and imaging devices for energy saving and environmental protection. On the other hand, ML directly establishes a relationship between the invisible mechanical forces and the visible optical signals without the requirement of circuit design, and hence it provides novel approaches and opportunities to achieve visualized and distributed sensing applications for large-area mechanics monitoring.[15–24]

To date, a large variety of material systems have been reported to have ML, which could be generally classified into three types based on the mechanics-induced morphological change of the materials, that is, the elastic-, plastic-, and fracture-ML.[25,26] Because of the non-destruction feature, elastic ML has attracted great attention during the past years, which provides the structural basis to produce recoverable ML for repeated use. However, most of the reported recoverable elastic-ML belongs to the trap-controlled type, generated from the electron transfer from the deep traps to the luminescent centers.[25,27,28] This process consumes the pre-stored energy, and requires UV/X-ray recharging for ML recovery,[29] which would seriously affect the practical operability. The self-activating ML is a direct excitation-emission process under mechanical stimuli.[30–34] It avoids light pre-irradiation (UV light or X-ray) to produce self-recoverable and repeatable ML, enabling sensors to achieve higher stability, reliability, and practicability. At present, the excited levels of the luminescent centers for the self-activating ML could gain energy via two approaches under mechanics, that is, excited by a

S. Qin, W. Wei, B. Tian, Z. Ma, Y. Wang, Z. Wang
State Key Laboratory of Solid Lubrication
Lanzhou Institute of Chemical Physics
Chinese Academy of Sciences
Lanzhou, Gansu 730000, P. R. China
E-mail: weiwy@licp.cas.cn; zhfwang@licp.cas.cn
B. Tian, S. Fang, Z. Wang
Shandong Laboratory of Advanced Materials and Green Manufacturing at Yantai
Yantai, Shandong 265503, P. R. China
B. Tian, J. Zhang
National & Local Joint Engineering Laboratory for Optical Conversion Materials and Technology
Lanzhou University
Lanzhou, Gansu 730000, P. R. China
E-mail: zhangjch@lzu.edu.cn
The ORCID identification number(s) for the author(s) of this article can be found under https://doi.org/10.1002/adfm.202401535

DOI: 10.1002/adfm.202401535

piezoelectric field or excited by an interfacial triboelectric field. As for being excited by the piezoelectric field, to the best of our knowledge, efficient, repeatable, and self-activating ML has only been reported in the system of transition metal-doped zinc sulfide with unclear underlying mechanisms.[13,35,36] Recently, an interfacial triboelectrification-based luminescent model was demonstrated, offering a series of self-activating and self-recoverable ML materials.[37–39] Although this model has been applied to many symmetric ML systems without piezoelectricity, these materials always require long self-recovery time (several hours or more), and cannot achieve repeated emission in continuous and rapid cyclic conditions (ML would disappear after only several or tens of continuous mechanics cycles).[38,40,41] Consequently, the development of self-activating and rapidly recoverable and repeatable ML materials with deep and clear physical insights is highly required.

The self-activating ML established from the interfacial triboelectrification should be realized by compositing the phosphor particles into a flexible matrix. Polydimethylsiloxane (PDMS) is the most employed polymer matrix because of its flexibility, transparency, and stress transfer ability.[14] Moreover, PDMS has been demonstrated to have strong negative charge affinity,[42,43] which always accepts electrons and exhibits high negative potential when rubbing with other materials.[37–39] Therefore, to achieve sensitive interfacial triboelectrification and efficient ML in the PDMS-based composites, the phosphor particles should be able to contribute electrons during rubbing. $Ca_6BaP_4O_{17}$ is a phosphate host with a monoclinic structure and a space group of *C2/m*.[44] In the structure of $Ca_6BaP_4O_{17}$, there are multiple cationic sites, that is, [BaO_{12}], [CaO_8], and [CaO_7] polyhedrons, which could facilitate the occupancies of rare earth ions and thus yielding various luminescence characteristics.[45,46] It is noticed that different from the conventional phosphates, there are unique and isolated O^{2-} ions in the structure of $Ca_6BaP_4O_{17}$, which may enhance the possibility of contributing electrons to generate triboelectrification when rubbing with PDMS.

Herein, in this work, we synthesized $Ca_6BaP_4O_{17}:Ce^{3+}$ (CBPOC) and fabricated the CBPOC/PDMS composite system. The employment of Ce^{3+} doping in this work is because of its well-known spin-allowed 4f-5d transitions for efficient absorption and emission.[47] The results suggest that we have successfully achieved the efficient self-activating ML modulated by the interfacial triboelectrification between the $Ca_6BaP_4O_{17}:0.02Ce^{3+}$ and PDMS. In addition, the $Ca_6BaP_4O_{17}:0.02Ce^{3+}$/PDMS composites simultaneously possess self-charging behavior. Under the cooperation of the self-activating and self-charging physical activities, the as-fabricated $Ca_6BaP_4O_{17}:0.02Ce^{3+}$/PDMS composites exhibit repeatable ML (ca. 1000 stretching cycles) with a fast self-recovery period (< 0.1 s), which further shows good thermal stability in a temperature range from 298 to 473 K. By utilizing the unique and attractive ML features of the developed $Ca_6BaP_4O_{17}:0.02Ce^{3+}$/PDMS composites, two types of intriguing devices in terms of the dual-information storage and photonic skin are further created, which show widespread applications in high-level information security, intelligent mechanics sensors, and human-machine interaction.

2. Results and Discussion

2.1. Basic Structure and Performance of CBPOC/PDMS Composites

As schemed in **Figure 1a**, we introduced CBPOC powders into the PDMS matrix to obtain high-performance interfacial triboelectrification-modulated self-activating ML materials. The CBPOC powders were synthesized by the solid-state method. As shown in Figure 1b, the crystal structure of CBPOC belongs to the monoclinic phase with *C2/m* space group, which is formed by packing of [BaO_{12}], [CaO_8], [CaO_7], and [PO_4] polyhedrons.[44] The X-ray diffraction patterns (XRD) patterns indicate that no obvious impurity phases have formed as a result of Ce^{3+} doping (Figure S1, Supporting Information). The CBPOC powders show irregular morphology with a size of 2 µm (Figure S2a, Supporting Information), and the Ca, Ba, P, O, and Ce have been uniformly distributed in the powders (Figure S2b, Supporting Information). When excited by 375 nm, the CBPOC powders exhibit photoluminescence (PL) peaks at 488 nm, attributing to the characteristic 5d→4f radiative transfers of Ce^{3+} (Figure S3, Supporting Information).[48]

The fabrication processes of CBPOC/PDMS are illustrated in Figure S4 (Supporting Information). The CBPOC:PDMS mass ratio was employed as 1:2, under which the as-fabricated CBPOC/PDMS could exhibit desirable ML performance and elastic properties (as shown in Figure S5, Supporting Information). The SEM images in Figure 1c,d display that the CBPOC microparticles are well dispersed in the PDMS matrix. The CBPOC microparticles could be wetted and closely adhered to by PDMS macromolecular chains, guaranteeing their good interfacial interactions with PDMS. Due to the fact that the addition of lubricating oil (PAO10) could reduce the friction between CBPOC powders and pure PDMS chains (Figure S6, Supporting Information), we added PAO10 into CBPOC/PDMS composites to investigate the influence on the ML performance. As shown in Figure 1e,f, the CBPOC/PDMS composite film could exhibit intense blue ML when stimulated by stretching with no pre-irradiation. However, the ML intensity of the composites is gradually decreased with the increased introduction of lubricating oil PAO10 into the structure, and the ML totally disappears when the oil content reaches 0.2 g. It should be noted that the addition of PAO10 shows almost no influence on the PL properties of the CBPOC (Figure S7, Supporting Information), which suggests that the PAO10 should neither be changing the intrinsic electron structure of the composites nor absorbing the emitted light. As a result, the significantly decreased ML intensity resulting from the introduction of PAO10 suggests that the interfacial friction/rubbing is critical to the ML performance of the CBPOC/PDMS composite structure. Figure 1g shows that the obvious ML signal could still be observed by the naked eye after 900 cycles of rapid and continuous stretching (frequency: 10 Hz). Compared to the initial intensity of the 1st cycle, the ML intensity of the CBPOC/PDMS is largely decreased. However, when the CBPOC/PDMS with decreased intensity is placed in the ambient environment for a long period, the ML intensity could be restored to a high level, for example, recovering to ca. 70% of the initial one

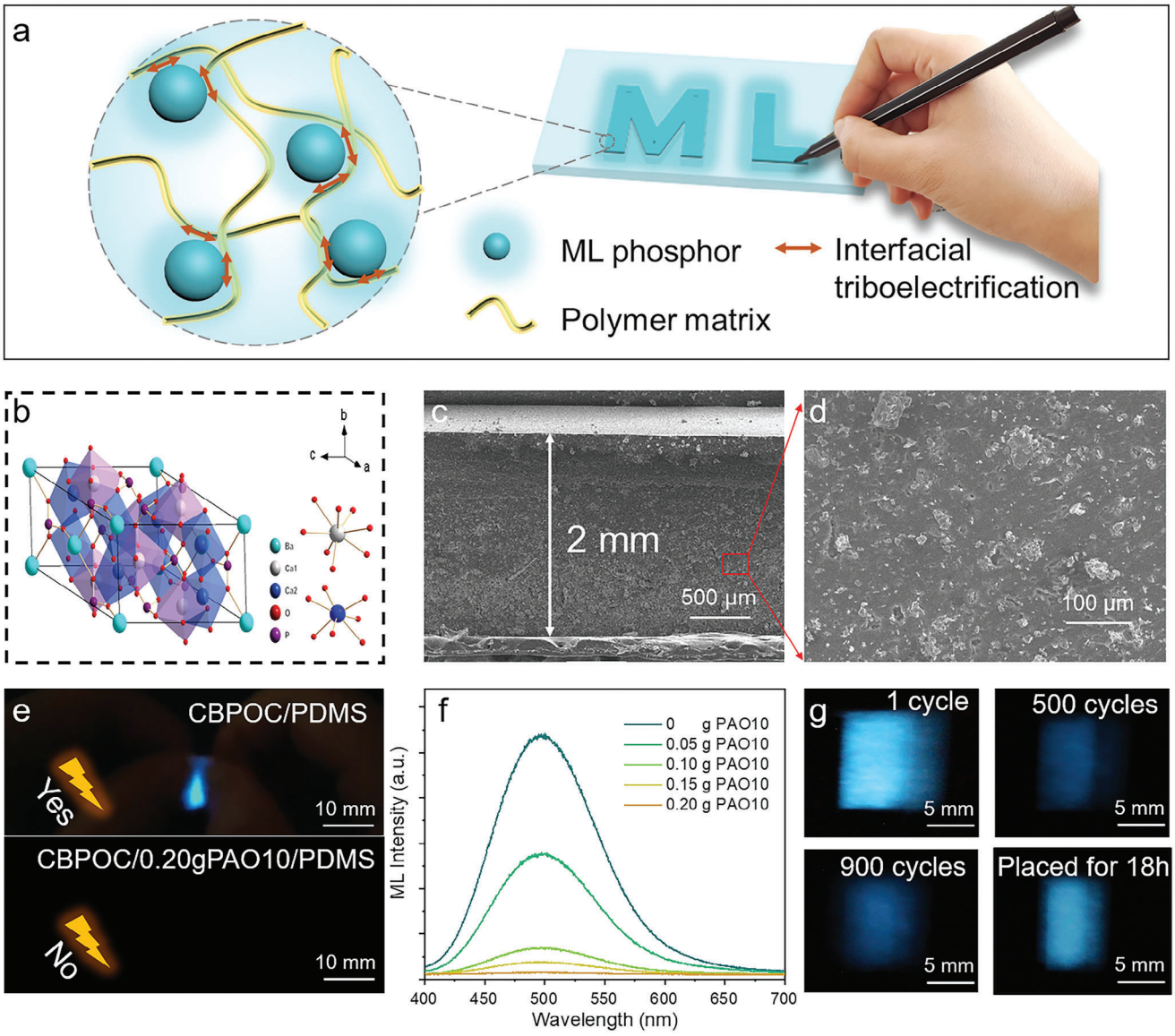

Figure 1. a) The schematic illustration of sensitive CBPOC/PDMS composite film. b) Crystal structure of the orthorhombic CBPOC. c,d) Cross-sectional scanning electron microscope (SEM) images of CBPOC/PDMS composite film. e) The ML photos of CBPOC/PDMS and CBPOC/PAO10/PDMS composite film under stretching. f) ML spectra of CBPOC/PDMS composite film with different PAO10 contents. g) Different tensile cycle ML photos and the one after placed for 18 h.

after placing 18 h. The above features of the CBPOC/PDMS are better than many of the reported symmetric ML materials (e.g., the $Sr_3Al_2O_5Cl_2$:Ln (Ln = Eu^{2+}, Tb^{3+}, Ce^{3+})/PDMS elastomers recovered ca. 40% and $Lu_3Al_5O_{12}$:Ce^{3+}/PDMS elastomers recovered 54% of initial intensity after placing 24 h at room temperature; the ML of the above two examples would disappear after only several continuous stretching cycles).[37,41] The self-recovery feature also suggests that the $Ca_6BaP_4O_{17}$:Ce^{3+}/PDMS could be repeatedly used with a higher ML intensity by prolonging the placement time or the time interval between the successive two cycles.

2.2. Self-Activating and Self-Charging Behaviors of CBPOC/PDMS Composites

The as-obtained ML from CBPOC/PDMS requires no pre-irradiation and can be stimulated at any time. Therefore, we have successfully achieved self-activating ML in CBPOC/PDMS, and the applied mechanics stimuli involve stretching, folding, rubbing, etc. (as exhibited in **Figure 2**a; Videos S1 and S2, Supporting Information). Figure 2b shows the self-activating ML spectra of CBPOC/PDMS composite with various Ce^{3+} ions doping concentrations under the tensile conditions (stretching strain: 100%;

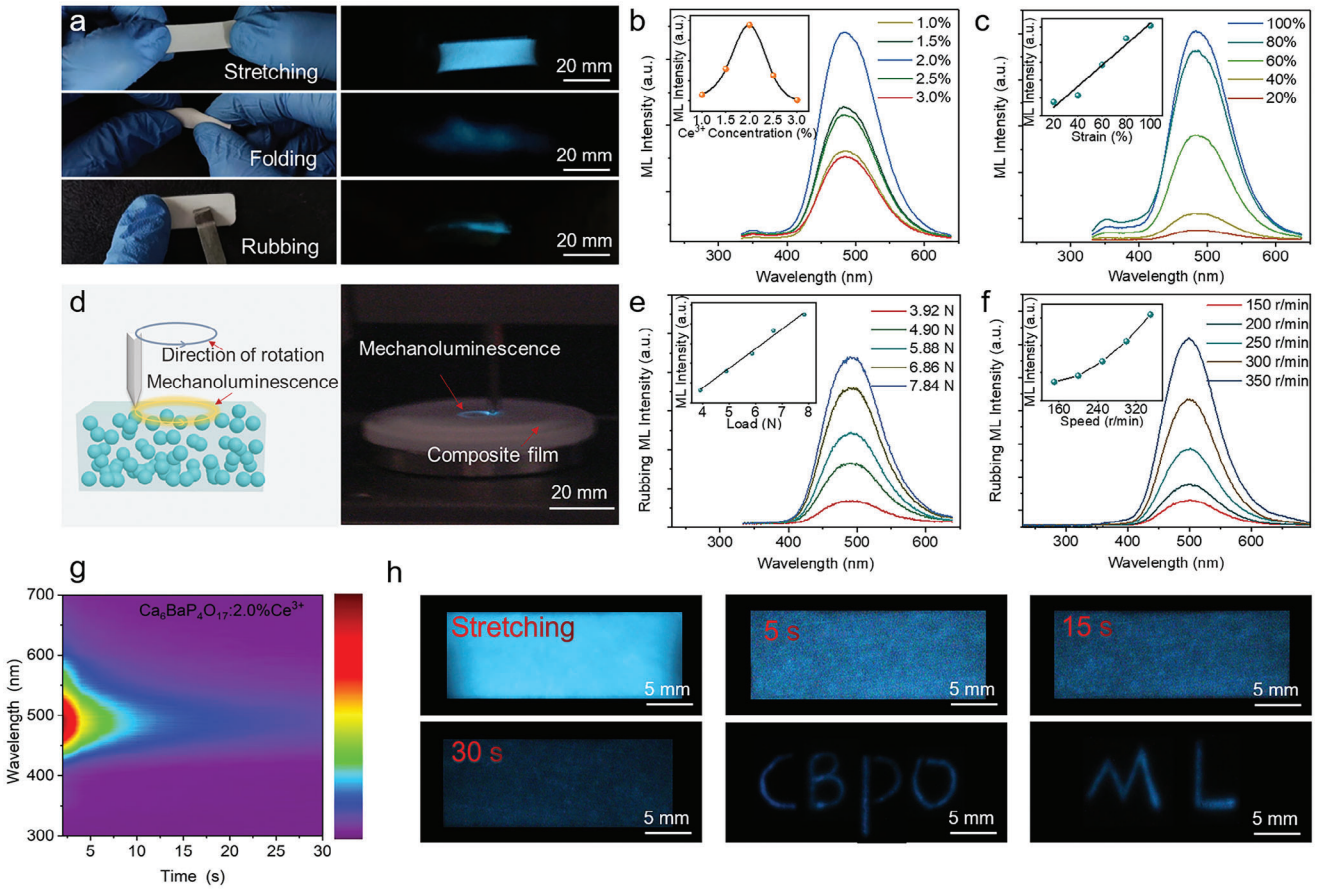

Figure 2. a) Optical and ML photographs of the as-fabricated CBPOC/PDMS composite film under stretching, folding, and rubbing stimuli, respectively. b) ML spectra and ML intensity of CBPOC/PDMS composite film with different Ce^{3+} doping concentrations. c) ML spectra and ML intensity variations under different stretching strains. d) The schematic illustration and the photo of $Ca_6BaP_4O_{17}$:0.02Ce^{3+}/PDMS composite film under a certain friction load. The friction-induced ML spectra and ML intensity variations versus **e** friction load and f) rotational speed of probe. g) Persistent ML mapping of $Ca_6BaP_4O_{17}$:0.02Ce^{3+}/PDMS composite film. h) ML afterglow photos of the $Ca_6BaP_4O_{17}$:0.02Ce^{3+}/PDMS after the stimuli of stretching for 0 to 30 s, and the photos of "CBPO" and "ML" displaying after writing. The ML intensity comparisons in the insets of b, c, e, and f were conducted using the maximum peak value by subtracting the background.

frequency: 4 Hz). With an increase in the Ce^{3+} content, the ML intensity initially rises and then falls due to the concentration quenching, and the ML signal exhibits the highest intensity at a concentration of 2.0 mol%. The composites all show light-blue ML with a main emission peak at 488 nm, possessing the same radiative transfer pathways as those of PL (Figure S3, Supporting Information). In addition, the mechanics responsiveness of the self-activating ML of the composites is investigated. As shown in Figure 2c, with the increase of the applied stretching strain from 20% to 100%, the self-activating ML intensity at 488 nm of the $Ca_6BaP_4O_{17}$:0.02Ce^{3+}/PDMS composite film increases accordingly. The ML intensity exhibits an approximately linear correlation to the applied strain with a sensitivity value of 59.635 ± 6.407. In addition to stretching, the stimulus-responsiveness behavior is also appropriate for the stimuli of rubbing or friction. Figure 2d presents the schematic illustration and the ML photo of the $Ca_6BaP_4O_{17}$:0.02Ce^{3+}/PDMS composite film under a certain friction load on the probe. The obvious friction trajectory and distribution could be visually observed by the naked eye. As shown in Figure 2e, with a fixed speed of 200 r min^{-1}, the increase of the applied friction load leads to an increased ML intensity with an approximately linear correlation (sensitivity value: 506.409 ± 27.459). Figure 2f presents a quadratic relationship between the ML intensity and the rotational speed when the friction load is set to 5.88 N. The increased ML intensity at higher rotational speed is possibly due to the enhanced wear rate of the composite film. Based on those relationships, the accurate load, rotational speed, and stretching strain could be easily read out by distinguishing/observing the ML brightness, and therefore the self-activating ML of the composite film is especially suitable for the visualized mechanics sensing in various areas.

Persistent ML with a long lifetime is highly necessitated to overcome the limitations of the transient emitting behavior under mechanical stimuli.[2,39,49,50] Herein, we further investigated the persistent ML properties of the as-fabricated CBPOC/PDMS composites with 2.0 mol% of Ce^{3+} doping. It is attractive to find that the $Ca_6BaP_4O_{17}$:0.02Ce^{3+}/PDMS composite film exhibits a long afterglow (30 s) after mechanics stimuli, with the persistent ML mapping illustrated in Figure 2g. The corresponding ML afterglow photos are presented in Figure 2h. Because the

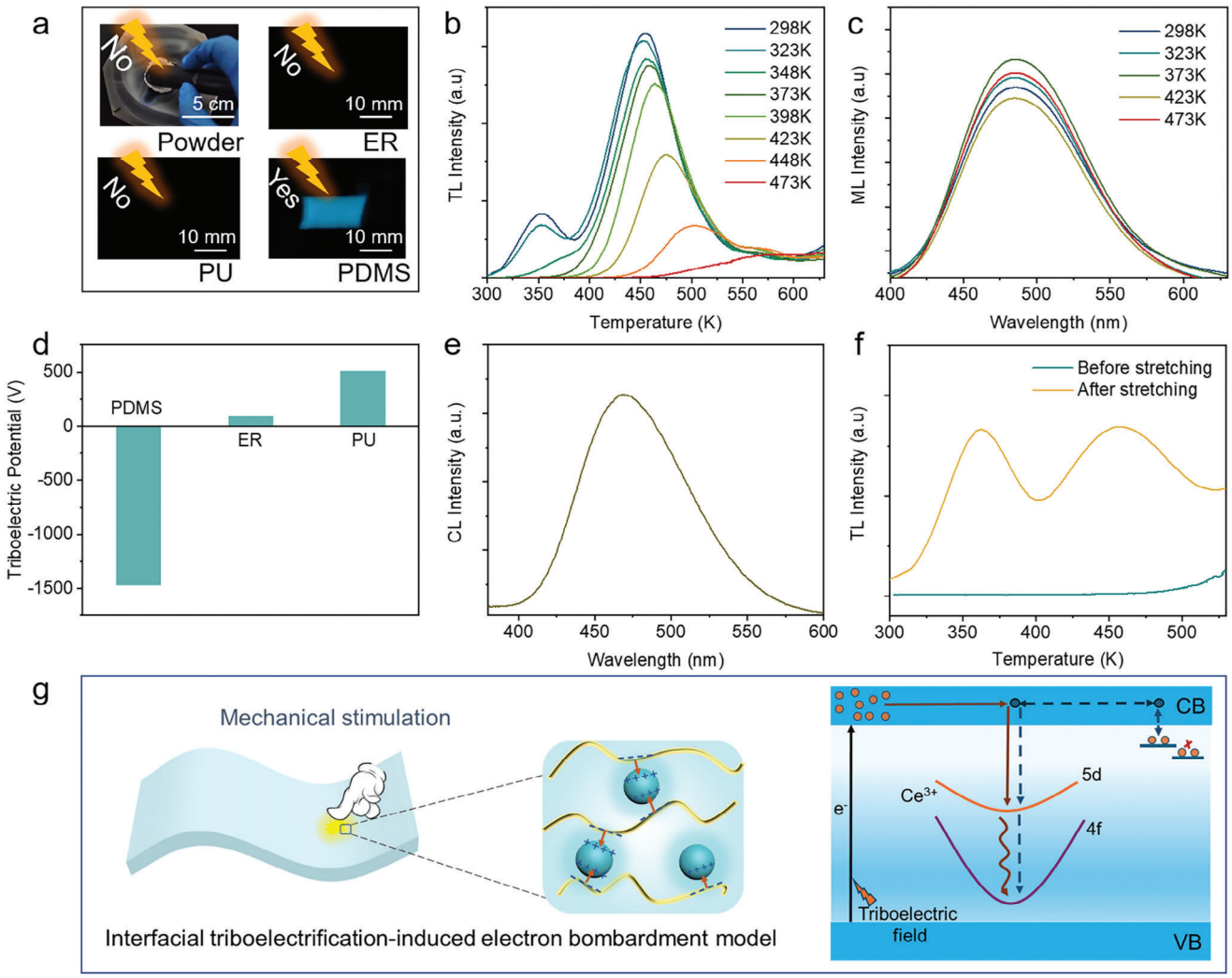

Figure 3. a) Illustration of the ML performance of $Ca_6BaP_4O_{17}$:0.02Ce^{3+} in various forms: powders and their composites with ER, PU, and PDMS, respectively. b) TL spectra of the pre-heat-treated $Ca_6BaP_4O_{17}$:0.02Ce^{3+}. c) ML spectra of the CBPOC/PDMS composite film with various pre-heat-treated $Ca_6BaP_4O_{17}$:0.02Ce^{3+}. d) Surface triboelectric potential of the polymer matrices when rubbing with $Ca_6BaP_4O_{17}$:0.02Ce^{3+} powders with 60 rpm under 1 N. e) CL spectrum of $Ca_6BaP_4O_{17}$:0.02Ce^{3+} powders. f) TL spectra of $Ca_6BaP_4O_{17}$:0.02Ce^{3+}/PDMS composite elastomers before and after stretching (stretching frequency: 4 Hz, stretching strain: 80%). g) Schematic diagram of the self-activating (solid line) and self-charging (dotted line) ML mechanisms of the CBPOC/PDMS composite elastomers.

generation of the persistent ML requires no pre-storing energy in the structure, it suggests that we have obtained a different type of persistent ML from the conventional one dependent on the deep traps.[2,49,50] Such kind of persistent ML is more convenient and valuable when operated in practical scenarios.

The ML of CBPOC is highly dependent on the matrices (**Figure 3a**). When the mechanical stimulations were applied to the CBPOC composited with hard epoxy resin (ER), no ML could be observed, confirming that the ML of CBPOC should be non-piezoelectricity-related. For the matrices in Figure 3a (ER, PU, and PDMS), only the CBPOC/PDMS composite film could exhibit the significant blue ML. The matrix effects on the ML behaviors of CBPOC suggest that the interfacial interactions between the CBPOC powders and the flexible polymer chains are critical, which is consistent with the results from the analysis of the addition of PAO10 lubricating oil (as discussed in Figure 1e,f).

Figure 3b,c shows the influence of the thermal treatment on the intrinsic trap structure and the ML intensity. With the increase of the treatment temperature from 298K to 473K, the TL (thermoluminescence) spectra are redshifted with the trapped carriers gradually cleared. However, the corresponding ML intensity of the composites exhibits a different variation (Figure 3c), and no obvious decrease in the ML intensity is observed, suggesting that the ML of the $Ca_6BaP_4O_{17}$:0.02Ce^{3+}/PDMS composite is independent of the deep traps. As a result, the classic ML models in terms of piezoelectricity and deep traps are inappropriate for the ML system in this work.

Recently, our group proposed a physical model to explain the peculiar self-activating ML in terms of interfacial triboelectrification-induced electron bombardment.[37–39] Figure 1e,f, suggests that the interfacial triboelectrification effect should play a crucial role in the ML performance of

CBPOC/PDMS composite film. Therefore, we use the four aspects proposed by previous research[37–39] to further verify whether it is suitable for this model: i) The ML is not related to piezoelectricity; ii) The ML is independent of traps; iii) There is triboelectrification between the ML powders and the matrices, and the electrons are transferred to the polymer chains (the electron transfer route directly determines the direction of the produced interfacial triboelectrification); iv) The ML has radiative routes when subjected to high energy electron bombardment. For the ML of CBPOC, it is unrelated to piezoelectricity (Figure 3a) and independent of traps (Figure 3b,c). When the CBPOC is rubbed with different matrices (Figure 3d), only the PDMS can accept electrons because of its strong negative charge affinity.[42,43] The $Ca_6BaP_4O_{17}$:0.02Ce^{3+} also exhibits obvious CL (cathodoluminescence) (Figure 3e), indicating that effective radiative routes exist when subjected to high-energy electron bombardment. Therefore, the ML of CBPOC in PDMS well meets the interfacial triboelectrification-induced electron bombardment model, which also explains why the addition of PAO10 oil significantly reduces the ML performance.

To further understand the persistent ML performance (Figure 2g,h), the TL spectra of $Ca_6BaP_4O_{17}$:0.02Ce^{3+}/PDMS composite film before and after stretching stimulus were measured. Before the measurement, the composite film is pre-heated to remove the electrons in traps. As shown in Figure 3f, the $Ca_6BaP_4O_{17}$:0.02Ce^{3+}/PDMS film exhibits no TL signal before stretching. However, after applying the stretching stimulus on the $Ca_6BaP_4O_{17}$:0.02Ce^{3+}/PDMS film, an obvious TL signal is obtained. It confirms that in addition to the self-activating ML, the $Ca_6BaP_4O_{17}$:0.02Ce^{3+}/PDMS also possesses self-charging behavior under mechanical stimulation. The mechanics-charged carriers in the shallow traps and their spontaneous transfer ability at room temperature are responsible for the as-observed persistent ML.

Based on the above results and discussion, the mechanisms for self-activating ML and self-charging persistent ML of CBPOC/PDMS are illustrated in Figure 3g. Under the mechanical stimuli, interfacial triboelectrification is formed between the CBPOC particles and the PDMS polymer chains, and the electrons are taken up by PDMS because of its strong negative charge affinity. Then, the accepted electrons in PDMS could be accelerated to bombard the CBPOC particles under the interfacial triboelectric field, which would cause the electron to be excited from the valence band (VB) to the conduction band (CB). The majority of the excited electrons in CB would transfer to the excited levels of Ce^{3+}, where they recombine with holes to produce the as-observed self-activating ML. The rest of the excited electrons could transfer from CB to traps to store energy, which is called self-charging. The self-charged (mechanics-charged) energy in the shallow traps could spontaneously transfer to the excited levels of Ce^{3+} after mechanical stimulus, producing the persistent ML or ML afterglow. From the above physical processes, it is known that the ML and persistent ML of the CBPOC/PDMS both belong to active activities and thus they require no pre-irradiation.

It should be noted that the CBPOC/PDMS could exhibit ML under various mechanics stimuli, for example, stretching, folding, and rubbing, as shown in Figure 2a. Although the different types of mechanics contain different stress information, the ML generation processes should be the same because all of these stimuli would induce a certain deformation to produce interfacial triboelectrification. The only difference of the ML under the stretching, rubbing, and folding modes should be the ML efficiency, among which the stretching mode is the most effective because of its largest deformation and consequently the highest degree of interfacial triboelectrification.

2.3. Repeatable, Self-Recoverable, and Thermally Stable ML of CBPOC/PDMS

Repeatability is one of the most important ML properties that could determine the service reliability and application scenarios. However, the majority of the ML materials have poor cyclic stability (ML totally disappears just after several or tens of rapid stretching cycles), or need external energy to charge for recovery and repeatable use, thus limiting the applications. To evaluate the ML cyclic stability or repeatability, the rubbing or the elastic compressing/stretching modes are mostly employed. Considering that the rubbing/friction process is always accompanied by the formation of new surfaces by damaging the composite films, the evaluation based on the elastic compressing/stretching mode is more reasonable and reliable. As far as we know, there is only one material at present, ZnS:Cu, which possesses the desirable ML cyclic stability and repeatability in PDMS under the cyclic elastic stretching mode.[33] Here, we report the oxide-based ML material that exhibits good self-recoverability, reproducibility, and stability under rapidly cyclic stretching conditions. As shown in **Figure 4a** and Videos S1 and S2 (Supporting Information), the ML signal of the composite is still visible to the naked eye after the continuous stretching (ca. 1000 stretching cycles). As the number of rapid stretching cycles increases, the blue ML signal gradually stabilizes after the initial drops which is consistent with the corresponding spectral signal change trend (Figure 4b,c; Figure S8, Supporting Information). Under the cyclic mechanics stimulation, the polymer matrix could exhibit a hysteresis effect where the deformation falls behind the stress,[51,52] and the interfacial rubbing action would be significantly decreased. Also, the weaker physical adsorption interactions between the CBPOC particles and the polymer network may break under stretching (Figure S9, Supporting Information). On unloading, the adsorption is varied, and the interfacial combination of the composite would be weakened.[53,54] In the composite film of $Ca_6BaP_4O_{17}$:0.02Ce^{3+}/PDMS, the hysteresis effect or adsorption variation is also suggested by the cyclic mechanical test, as shown in Figure S10 (Supporting Information), which would reduce the interfacial interactions between the ML particles and polymer network. Therefore, the interfacial triboelectric field would be decreased, resulting in reduced self-activating ML intensity at the initial stage. When the rapid stretching cycles are >300 times, the interfacial interactions of ML particles and polymer chains reach balance, leading to a stable self-activating ML signal output with a 99.98% self-recovery degree to the last cycle (Figure 4c). The applied 10 Hz stretching condition suggests that the single stretching and releasing period, plus the short time interval between the successive two cycles should be 0.1 s in total. Therefore, the exact period of the 99.98% self-recovery should be < 0.1 s. As for the attractive ML repeatability of the $Ca_6BaP_4O_{17}$:0.02Ce^{3+}/PDMS, the unique structure of the CBPOC with isolated O^{2-} and the strong

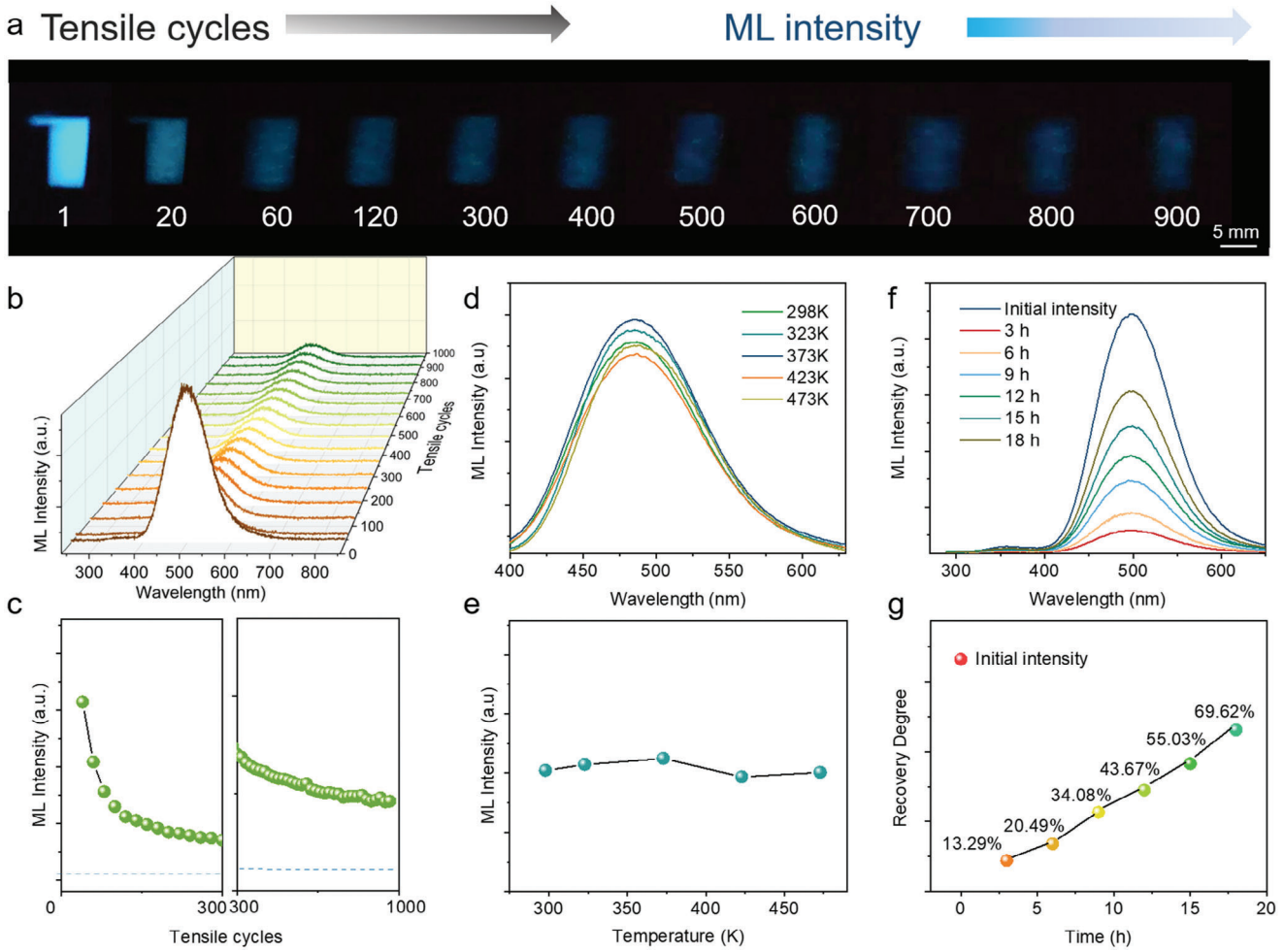

Figure 4. a) The ML photos of $Ca_6BaP_4O_{17}$:0.02Ce^{3+}/PDMS under different tensile cycles. b,c) The repeatability and cyclic stability of the composite film exposed to a repeating mechanical stretching test. The repeatability tests were performed under a strain of 80% at a frequency of 10 Hz, and the ML spectra/intensity were collected from the 20th to 960th stretching cycles with an integration time of 2 s. d) ML spectra and e) ML intensity changes of $Ca_6BaP_4O_{17}$:0.02Ce^{3+}/PDMS composite film under various ambient temperatures. f,g) The ML recovery degree of the $Ca_6BaP_4O_{17}$:0.02Ce^{3+}/PDMS elastomers at room temperature compared with the initial intensity (the one at 1st cycle).

negative charge affinity of PDMS should be basically responsible for this activity. Moreover, the unique self-charging processes could also facilitate the repeatable process of self-activating ML, because the self-stored mechanical energy in the shallow traps could be further converted into light emission in the next mechanical stimulus cycle. It should be noted that although the ML intensity at the initial cyclic stage (0–300 cycles) declined sharply, the stabilized ML signal after 300 cycles is still visible to the naked eye, which breaks through the current limitations of the oxide-based ML materials. Future improvements on the fatigue damage of the PDMS structure and the self-repair of the $Ca_6BaP_4O_{17}$:0.02Ce^{3+}-PDMS interfaces are promising to further enhance the stabilized ML intensity/brightness.

In addition to the cyclic stability, the ML of the $Ca_6BaP_4O_{17}$:0.02Ce^{3+}/PDMS composite film also exhibits good thermal stability. As shown in Figure 4d,e, the $Ca_6BaP_4O_{17}$:0.02Ce^{3+}/PDMS shows a stable ML that is insusceptible to the surrounding temperature, which should be the comprehensive result from the variations of the non-radiative transfer rate, interfacial triboelectric field, and its charge decay rate.[37] Another intriguing feature of $Ca_6BaP_4O_{17}$:0.02Ce^{3+}/PDMS composite film is its structure restore ability. Although the ML intensity is stabilized with a 99.98% self-recovery degree to the last cycle and a short self-recovery period of < 0.1 s under the rapid and continuous stretching stimuli, it is still far below the initial one of the 1st cycle. Because the elastic lag and interfacial combination could be gradually alleviated or repaired by increasing the placement time, the ML spectra of the resulted films under various placement times were collected to show the structure restore property. An attractive phenomenon is that the ML restore degree increases as the placement time increases (Figure 4f,g). When the placement time is extended to 18 h at room temperature, the ML could return to 69.62% of its initial intensity (the one at 1st cycle). This property suggests that the stabilized and repeated ML in this work could be enhanced to a higher level by prolonging the placement time or the time interval between the successive two cycles. This may further promote the performance exhibition of the repeatable ML.

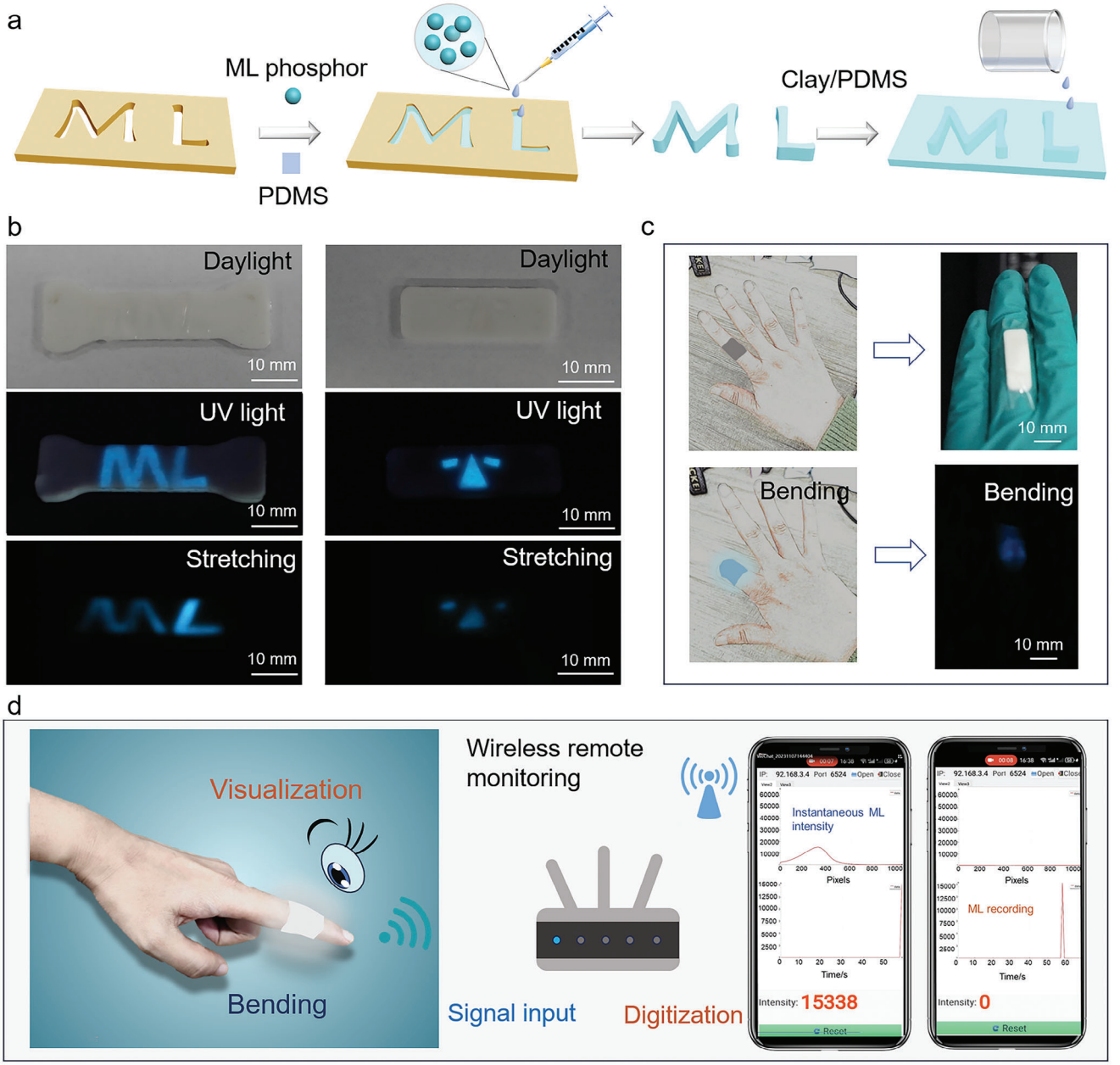

Figure 5. a) Fabricating processes of the dual-mode information storage and encryption device. b) Optical photographs of the information storage and encryption patterns under different activations/stimulations. c) Schematics and optical photographs of the photonic skin. d) Wireless monitoring and recording of the bending-induced ML signals of the photonic skin on the smartphone.

2.4. Device Applications

The developed $Ca_6BaP_4O_{17}$:0.02Ce^{3+}/PDMS composite overcomes the repeatable, self-recoverable, and stable problems in conventional ML systems, which exhibit great advantages for device applications. Here, we propose the dual-mode information storage and encryption device application to demonstrate the high performance of $Ca_6BaP_4O_{17}$:0.02Ce^{3+}/PDMS composite film. **Figure** 5a illustrates the fabrication processes. The fabricated device contains the ML pre-written region with the composition of $Ca_6BaP_4O_{17}$:0.02Ce^{3+}/PDMS, and the rest region is filled with clay/PDMS. Under daylight, the entire device shows a uniform off-white color with no information revealed. When placed under 365 nm UV light or stretched the device under dark conditions, the pre-written patterns in the device could be displayed and observed (Figure 5b; Video S3, Supporting Information). By changing the pre-written patterns, various information could be written in and read out. The developed information storage and encryption device not only allows the dual-mode stimulations in terms of the UV light and the mechanics to decode the information, but also has high stability and reliability because of the self-activating and self-charging ML behaviors.

Considering the human skin's sensing features and the mechanic's responsiveness of the ML composites, we further apply the $Ca_6BaP_4O_{17}$:0.02Ce^{3+}/PDMS film as photonic skin on a human joint to demonstrate the skin-driven ML exhibition. As shown in Figure 5c, when the $Ca_6BaP_4O_{17}$:0.02Ce^{3+}/PDMS film is attached to the finger joint and the bending activity is applied, an obvious intense blue ML signal is observed, which shows an elementary linear relationship with the joint bending degree (Figure S11, Supporting Information). The bending-induced ML signals could also be wirelessly monitored and recorded by a smartphone (as shown in Figure 5d). Moreover, the as-fabricated photonic skin is soft and flexible (Figure S12, Supporting Information) with an appropriate friction coefficient (μ: ca. 0.4) when rubbing against the artificial leather (Figure S13, Supporting Information), suggesting its conformability to human skin. Therefore, the as-fabricated $Ca_6BaP_4O_{17}$:0.02Ce^{3+}/PDMS-based photonic skin shows high application values for intelligent artificial skin and human-machine interaction.

3. Conclusion

In summary, the self-activating ML system of $Ca_6BaP_4O_{17}$:0.02Ce^{3+}/PDMS modulated by interfacial triboelectrification was developed. It not only emits intense self-activating blue ML in response to rubbing or stretching with no need for pre-irradiation but also possesses self-charging behavior. Accordingly, the as-fabricated $Ca_6BaP_4O_{17}$:0.02Ce^{3+}/PDMS composites exhibit thermally stable and repeatable ML (ca. 1000 stretching cycles) with a fast self-recovery period (< 0.1 s). The unique and attractive ML features further endow the $Ca_6BaP_4O_{17}$:0.02Ce^{3+}/PDMS potential applications in dual-mode information storage and photonic skin. Overall, this work offers a comprehensive and in-depth investigation of the self-recoverable, highly repeatable, and thermally stable ML, which shows high guiding values for future ML design and applications.

4. Experimental Section

Materials: $CaCO_3$ was purchased from Meryer. $NH_4H_2PO_4$, $BaCO_3$, and CeO_2 were purchased from Aladdin. All commercial reagents and solvents were used without additional purification. PDMS of Sylgard®184 was purchased from Dow Corning.

Synthesis of CBPOC Powders: A series of $Ca_6BaP_4O_{17}$:$x$$Ce^{3+}$ (x = 1.0%, 1.5%, 2.0%, 2.5%, 3.0%) powders were synthesized by a high-temperature solid-state method. First, stoichiometric amounts of $CaCO_3$, $BaCO_3$, $NH_4H_2PO_4$, and CeO_2 raw materials were weighed and thoroughly ground in an agate mortar. Then, the mixture was sintered at 1280 °C for 10 h under the atmosphere of 95% N_2 and 5% H_2 in a tube furnace. After cooling to room temperature, the $Ca_6BaP_4O_{17}$:Ce^{3+} powders were obtained by grinding.

Fabrication of CBPOC/PDMS Composites: PDMS base resin (2.0 g) and curing agent (0.2 g) with a mass ratio of 10:1 were mixed in a petri dish (diameter: 30 mm). Then, 1.0 g of CBPOC powders were dispersed homogeneously into the above PDMS precursor by mechanical stirring for 10 min. After that, the mixture was poured into a dumbbell-shaped polytetrafluoroethylene (PTFE) mold (25 mm × 10 mm × 2 mm) and kept under negative pressure (−80 kPa) for 30 min to remove the gas. After curing at 70 °C for 1 h, standard test samples of CBPOC/PDMS composite elastomers were obtained. For comparison, CBPOC/PU and CBPOC/ER composites were also fabricated, and the preparation processes were similar to those of CBPOC/PDMS. The ratios of base resin to curing agent and powders for CBPOC/PU and CBPOC/ER were set as 1:1:2 and 3:1:1, respectively.

Fabrication of Dual-Mode Information Storage Device: First, a polylactic acid mold with two letters of "ML" was printed by a 3D printer. Meanwhile, 0.5 g of $Ca_6BaP_4O_{17}$:0.02Ce^{3+} was mixed with PDMS base resin (1.0 g) and curing agent (0.1 g) by mechanical stirring. Then, the mixture was transferred into the 3D-printed mold. After curing in the oven at 70 °C for 1 h, the two cured letters "M" and "L" were molded and placed in a rectangular PTFE mold. After filling a mixture of clay (0.2 g), base resin (1.0 g), and curing agent (0.1 g) in the rest area, and further curing at 70 °C for 1 h, the dual-mode information storage device was achieved.

Characterizations: The XRD patterns were performed on XRD-6100 (Shimadzu. Japan) X-ray diffractometer with $Cu_{K\alpha}$ radiation (λ = 1.54178 Å). The morphology and element distribution of the samples were obtained by SEM (Tecnai-G2-F30) equipped with energy-dispersive X-ray spectroscope fittings (EDAX ELEMENT). The PL and PL excitation spectra were measured from an Omniλ300i fluorescence spectrometer with an excitation source of a 500 W Xe 900 lamp. The ML spectra were obtained from the above spectrophotometer by further equipping with a CCD camera (iVac-316, Edmund Optics Ltd.). A uniaxial tensile test was carried out on a universal tensile machine (Shimadzu AGS-X-10 kN) at a strain rate of 100 mm min^{-1} at room temperature. The Tribological performance test was performed by MS-T3001 (Lanzhou Huahui Instrument Technology Co., Ltd.). ML signals were collected from a homemade tensile testing machine using a high-throughput optical fiber. The TL curves were measured using a microcomputer thermoluminescence spectrometer (FJ427A1, Beijing Nuclear Instrument Factory) at a heating rate of 1 K s^{-1}. The triboelectric potential was measured using the electrostatic measuring probe (SK050, KEYENCE (Japan) Co., Ltd.) at a distance of 10 mm. The CL spectrum was detected on the modified Mp-Micro-S instrument attached to the SEM. All optical photos were taken by a digital camera (Canon EOS 77D) at room temperature.

Human Participant Statement: Before the experiments, the voluntarily participating human object gave the written consent form. The volunteer bent the CPBOC/PDMS film by her finger joint to demonstrate the skin-driven ML exhibition, and there was no physiological or psychological effect on the volunteer. All experiments with human participants were conducted in compliance with relevant laws, and approved by the Ethics Committee of Lanzhou Institute of Chemical Physics, Chinese Academy of Sciences.

Statistical Analysis: All data were processed by Origin software (Version 2021). The data on ML intensity was obtained from the highest point of the emission peak. For the comparison of ML intensity, the background intensity was subtracted.

Supporting Information

Supporting Information is available from the Wiley Online Library or from the author.

Acknowledgements

This work was supported by the Strategic Priority Research Program of the Chinese Academy of Sciences (XDB 0470201), the National Natural Science Foundation of China (12074159), the Natural Science Foundation of Gansu Province (23JRRA647 and 23JRRA646), the Natural Science Foundation for Distinguished Young Scholars of Gansu Province (20JR5RA572), the Shandong Province Natural Science Foundation (ZR2023QB249), the Regional Development Young Scholar Program of the Chinese Academy of Sciences (E30283YRC1), and the Taishan Scholars Program.

Conflict of Interest

The authors declare no conflict of interest.

Data Availability Statement

The data that support the findings of this study are available from the corresponding author upon reasonable request.

Keywords

information storage, mechanoluminescence, photonic skin, repeatability, self-recovery

Received: January 25, 2024
Revised: March 21, 2024
Published online:

[1] S. M. Jeong, S. Song, S.-K. Lee, N. Y. Ha, *Adv. Mater.* **2013**, *25*, 6194.
[2] B. Tian, Z. Wang, A. T. Smith, Y. Bai, J. Li, N. Zhang, Z. Xue, L. Sun, *Nano Energy* **2021**, *83*, 105860.
[3] Z. Ma, J. Zhou, J. Zhang, S. Zeng, H. Zhou, A. T. Smith, W. Wang, L. Sun, Z. Wang, *Mater. Horiz.* **2019**, *6*, 2003.
[4] P. Zhou, Q. Zhang, F. Peng, B. Sun, X. Dou, B. Liu, D. Han, Y. Xue, K. Ding, *J. Rare Earths* **2022**, *40*, 870.
[5] Y. Wang, W. Yang, H. Chen, X. Zhong, G. Zeng, Y. Li, C. Hou, *Faguang Xuebao* **2022**, *43*, 1609.
[6] Y. Du, Y. Jiang, T. Sun, J. Zhao, B. Huang, D. Peng, F. Wang, *Adv. Mater.* **2019**, *31*, 1807062.
[7] D. Tu, C.-N. Xu, A. Yoshida, M. Fujihala, J. Hirotsu, X.-G. Zheng, *Adv. Mater.* **2017**, *29*, 1606914.
[8] H. Suo, Y. Wang, X. Zhang, W. Zheng, Y. Guo, L. Li, P. Li, Y. Yang, Z. Wang, F. Wang, *Matter* **2023**, *6*, 2935.
[9] R. R. Petit, S. E. Michels, A. Feng, P. F. Smet, *Light Sci Appl* **2019**, *8*, 124.
[10] Y. Zhao, D. Peng, G. Bai, Y. Huang, S. Xu, J. Hao, *Adv. Funct. Mater.* **2021**, *31*, 2010265.
[11] J. S. Kim, G.-W. Kim, *Sens. Actuators, A* **2014**, *218*, 125.
[12] X. Qian, Z. Cai, M. Su, F. Li, W. Fang, Y. Li, X. Zhou, Q. Li, X. Feng, W. Li, X. Hu, X. Wang, C. Pan, Y. Song, *Adv. Mater.* **2018**, *30*, 1800291.
[13] B. Zhou, J. Liu, X. Huang, X. Qiu, X. Yang, H. Shao, C. Tang, X. Zhang, *Nano-Micro Lett.* **2023**, *15*, 72.
[14] S. M. Jeong, S. Song, K.-I. Joo, J. Kim, S.-H. Hwang, J. Jeong, H. Kim, *Energy Environ. Sci.* **2014**, *7*, 3338.
[15] L. Liu, C.-N. Xu, A. Yoshida, D. Tu, N. Ueno, S. Kainuma, *Adv. Mater. Technol.* **2019**, *4*, 1800336.
[16] Y. Kim, J.-S. Kim, G.-W. Kim, *Sci. Rep.* **2018**, *8*, 12023.
[17] B. Hou, L. Yi, C. Li, H. Zhao, R. Zhang, B. Zhou, X. Liu, *Nat. Electronics* **2022**, *5*, 682.
[18] W. Yang, W. Gong, W. Gu, Z. Liu, C. Hou, Y. Li, Q. Zhang, H. Wang, *Adv. Mater.* **2021**, *33*, 2104681.
[19] Y. Xie, Z. Li, *Chem* **2018**, *4*, 943.
[20] D. Tu, C.-N. Xu, S. Kamimura, Y. Horibe, H. Oshiro, L. Zhang, Y. Ishii, K. Hyodo, G. Marriott, N. Ueno, X.-G. Zheng, *Adv. Mater.* **2020**, *32*, 1908083.
[21] J.-C. Zhang, C.-N. Xu, S. Kamimura, Y. Terasawa, H. Yamada, X. Wang, *Opt. Express* **2013**, *21*, 12976.
[22] J. S. Kim, Y.-N. Kwon, N. Shin, K.-S. Sohn, *Acta Mater.* **2005**, *53*, 4337.
[23] C. Chen, Z. Lin, H. Huang, X. Pan, T.-L. Zhou, H. Luo, L. Jin, D. Peng, J. Xu, Y. Zhuang, R.-J. Xie, *Adv. Funct. Mater.* **2023**, *33*, 2304917.
[24] Z. Liu, X. Yu, Q. Peng, X. Zhu, J. Xiao, J. Xu, S. Jiang, J. Qiu, X. Xu, *Adv. Funct. Mater.* **2023**, *33*, 2214497.
[25] J.-C. Zhang, X. Wang, G. Marriott, C.-N. Xu, *Prog. Mater. Sci.* **2019**, *103*, 678.
[26] Y. Zhuang, R.-J. Xie, *Adv. Mater.* **2021**, *33*, 2005925.
[27] D. Tu, C.-N. Xu, Y. Fujio, A. Yoshida, *Light Sci Appl* **2015**, *4*, e356.
[28] C. Chen, Y. Zhuang, D. Tu, X. Wang, C. Pan, R.-J. Xie, *Nano Energy* **2020**, *68*, 104329.
[29] B. Chen, X. Zhang, F. Wang, *Acc Mater Res* **2021**, *2*, 364.
[30] J. Ning, Y. Zheng, Y. Ren, L. Li, X. Shi, D. Peng, Y. Yang, *Sci. Bull.* **2022**, *67*, 707.
[31] D. Peng, Y. Jiang, B. Huang, Y. Du, J. Zhao, X. Zhang, R. Ma, S. Golovynskyi, B. Chen, F. Wang, *Adv. Mater.* **2020**, *32*, 1907747.
[32] C. N. Xu, T. Watanabe, M. Akiyama, X. G. Zheng, *Appl. Phys. Lett.* **1999**, *74*, 1236.
[33] S. M. Jeong, S. Song, S.-K. Lee, B. Choi, *Appl. Phys. Lett.* **2013**, *102*, 051110.
[34] W. Wang, Z. Wang, J. Zhang, J. Zhou, W. Dong, Y. Wang, *Nano Energy* **2022**, *94*, 106920.
[35] X. Wang, H. Zhang, R. Yu, L. Dong, D. Peng, A. Zhang, Y. Zhang, H. Liu, C. Pan, Z. L. Wang, *Adv. Mater.* **2015**, *27*, 2324.
[36] M. V. Mukhina, J. Tresback, J. C. Ondry, A. Akey, A. P. Alivisatos, N. Kleckner, *ACS Nano* **2021**, *15*, 4115.
[37] Y. Bai, F. Wang, L. Zhang, D. Wang, Y. Liang, S. Yang, Z. Wang, *Nano Energy* **2022**, *96*, 107075.
[38] Z. Ma, Y. Han, Y. Bai, B. Liu, Z. Wang, *Chem. Eng. J.* **2023**, *456*, 141122.
[39] Y. Bai, X. Guo, B. Tian, Y. Liang, D. Peng, Z. Wang, *Adv. Sci.* **2022**, *9*, 2203249.
[40] J. Zhou, Y. Gu, J. Lu, L. Xu, J. Zhang, D. Wang, W. Wang, *Chem. Eng. J.* **2020**, *390*, 124473.
[41] P. Zhang, J. Wu, L. Zhao, Z. Guo, H. Tang, Z. Wang, Z. Liu, W. Chen, X. Xu, *ACS Sustainable Chem. Eng.* **2023**, *11*, 4073.
[42] J. Chen, Z. L. Wang, *Joule* **2017**, *1*, 480.
[43] Y. Liu, J. Mo, Q. Fu, Y. Lu, N. Zhang, S. Wang, S. Nie, *Adv. Funct. Mater.* **2020**, *30*, 2004714.
[44] N. Komuro, M. Mikami, Y. Shimomura, E. G. Bithell, A. K. Cheetham, *J. Mater. Chem. C* **2014**, *2*, 6084.
[45] N. Komuro, M. Mikami, Y. Shimomura, E. G. Bithell, A. K. Cheetham, *J. Mater. Chem. C* **2015**, *3*, 204.
[46] R. Zhou, C. Liu, L. Lin, Y. Huang, H. Liang, *Chem. Eng. J.* **2019**, *369*, 376.
[47] P. Li, Z. Wang, Z. Yang, Q. Guo, X. Li, *J. Lumin.* **2010**, *130*, 222.
[48] L. Ning, X. Huang, J. Sun, S. Huang, M. Chen, Z. Xia, Y. Huang, *J. Phys. Chem.* **2016**, *120*, 3999.
[49] J. Botterman, K. V. d. Eeckhout, I. D. Baere, D. Poelman, P. F. Smet, *Acta Mater.* **2012**, *60*, 5494.
[50] N. Zhang, B. Tian, Z. Wang, A. T. Smith, Z. Ma, Z. Xue, L. Sun, *Adv. Opt. Mater.* **2021**, *9*, 2100137.
[51] X. Guo, J. Bian, Y. Bai, Z. Ma, S. Yang, Z. Wang, *Chem. Phys. Lett.* **2022**, *787*, 139235.
[52] Z. Wang, C. Xiang, X. Yao, P. L. Floch, J. Mendez, Z. Suo, *Proc. Natl. Acad. Sci. USA* **2019**, *116*, 5967.
[53] J. M. Clough, C. Creton, S. L. Craig, R. P. Sijbesma, *Adv. Funct. Mater.* **2016**, *26*, 9063.
[54] M. A. Kashfipour, N. Mehra, J. Zhu, *Adv. Compos. Hybrid Mater.* **2018**, *1*, 415.